Hindawi
Advances in Civil Engineering
Volume 2024, Article ID 9994801, 15 pages
https://doi.org/10.1155/2024/9994801

*Research Article*

# Reasonable Treatment Range of Karst Cave Encountered by Super-Large Diameter Shield Tunnel in Strongly Karst-Developed Area

**Jiang Wang**,[1,2] **Jinwen Yang**,[1] **and Xianglin Yan**[1]

[1]*China Railway 16th Bureau Group Co., Ltd., Beijing 100018, China*
[2]*Faculty of Architecture, Civil and Transportation Engineering, Beijing University of Technology, Beijing 100124, China*

Correspondence should be addressed to Jiang Wang; 16115290@bjtu.edu.cn

Received 9 January 2023; Revised 13 August 2023; Accepted 20 December 2023; Published 11 March 2024

Academic Editor: Valeria Vignali



When a super-large diameter shield tunnel passes through a strongly karst-developed area, in order to ensure the stability of the tunnel and economy of karst reinforcement, the reasonable treatment range for a huge number of karst caves needs to be researched. Based on a karst treatment project of a shield tunnel with a diameter of 14.5 m, this paper studies the influence of intrusive fully filled karst caves on the stability of the lining and excavation face by using theoretical calculation. In addition, the safe distance between the tunnel and karst caves outside the tunnel is proposed through numerical simulation, and the corresponding treatment range is obtained. The results show that the bearing capacity of the lining has a certain reserve when the intrusive cave is smaller than a certain size, and the caves filled with plastic or hard plastic clay have sufficient antifracturing ability. Therefore, some small fully filled caves inside the tunnel profile can be left unreinforced. On the other side, the critical safe distance is only 1–2 m for the caves with a size of 3 m, so the outside caves with a size less than 3 m can be left unreinforced in the treatment range farther away from the tunnel. The proposed treatment range is close to similar projects that have been built, indicating that analysis results are reasonable.

## 1. Introduction

With the development and utilization of the urban underground space, a large number of shield tunnels run through the karst geological areas. Most of the typical karst products such as karst caves are extremely concealing, which can easily induce engineering disasters including shield machine head drooping, surface karst collapse, water inrush, and so on [1]. Therefore, it is no exaggeration that the karst caves have become a serious threat to shield tunnel excavation projects [2, 3]. Furthermore, the number of encountered karst caves is huge for super-large diameter shield tunnels in strongly karst-developed strata, and the tunnel construction faces a greater threat. In order to deal with these threats, karst caves that have high collapse potential need to be treated prior to the tunnel construction [4]. Hence, the reasonable treatment range must be determined considering the stability of the tunnel and the cost of the karst cave treatment.

In the current study about shield tunnels, a tunnel diameter of 6–8 m is generally defined as a medium diameter [5], a tunnel diameter of 8–12 m is defined as a large diameter, and a tunnel diameter of more than 12 m is defined as a super-large diameter [5–7]. A lot of research has focused on the treatment range of medium-diameter shield tunnels, including theoretical analysis [8–11], empirical analogy [12–17], and numerical simulation [18, 19]. Sun [8] and Liu et al. [9] deduced a formula for the safe distance between karst caves and the tunnel by using the limit analysis upper bound method, and the treatment range was calculated based on a shield tunnel project of Jinan metro. Li et al. [10] determined the treatment range of the different types of karst caves for a cross-sea shield tunnel of Dalian metro line 5, combined with the analysis of the grouting reinforcement and collapsed arch. Based on a shield tunnel project of Changsha metro line 1, Long [11] estimated the safe thickness of the rock mass between karst caves and the tunnel by the approximate

analysis method of the structural mechanics. In terms of the empirical analogy, most of the studies are based on similar engineering cases in specific areas to explore the size of the treatment range. According to the engineering conditions and relevant specifications, the scholars formulated the treatment principles of karst caves for shield tunnels, and then the treatment range was put forward by referring to the construction experience of each region [12–17]. In terms of the numerical simulation, Wang et al. [18] used FLAC3D to study the influence of geometric parameters and filling degree of karst caves on the safe thickness of the rock mass, and a safe distance prediction model for Wuhan metro line 6 was obtained. Based on a shield tunnel project in Nanning, Xie [19] applied numerical simulation to analyze the effect of some parameters on the safe distance between karst caves and the tunnel.

In general, the safe distance for the caves outside the tunnel can be determined by a simplified method of structural mechanics or numerical simulation. Furthermore, the treatment range was usually determined by the safe distance. However, the above method ignores the effect of the caves intruding into tunnels, and the intrusive caves within the obtained range are required to be treated. At present, there are few reports about the treatment range of super-large diameter shield tunnels.

Table 1 summarizes the treatment range from previous studies [14, 19–23]. As can be seen in Table 1, the bottom boundary of the treatment range is mostly $1.0D$ ($D$ is the outer diameter of the tunnel) away from the tunnel profile, other boundaries are $0.5D$ away from the tunnel profile, and caves within the range must be reinforced. This treatment range is also adopted for some large diameter shield tunnels [24].

This paper is based on a karst treatment project of the shield tunnel with a diameter of 14.5 m located in strongly karst-developed strata. With reference to the abovementioned treatment range, the number of reinforced caves in the background project of this paper will exceed 700. If the drilling of grouting reinforcement is carried out at 2 m intervals, the total drilling length reaches 300,000 m, which will cost a lot in the process of karst cave reinforcement.

For some small fully filled karst caves, even if they intrude into the tunnel, the stability of shield linings is less affected [25–27]. In addition, karst caves have little effect on the stability of surrounding rock when the thickness of the rock mass between the shield tunnel and karst caves is sufficient [8–11, 19, 20]. The cost of reinforcement can be effectively reduced when the karst caves of the above two types are not treated (Figure 1). In this regard, this paper analyzes the influence of fully filled caves intruding into the tunnel and caves outside the tunnel. Then, the type of caves that can be nontreated and a reasonable treatment range is studied for a super-large diameter shield tunnel.

## 2. Project Overview

*2.1. Introduction to Project.* The lining of a super-large diameter shield tunnel in Wuhan has an inner diameter of 13.3 m, an outer diameter of 14.5 m, a ring width of 2 m, and a ring thickness of 0.6 m. The slurry shield with a diameter of 15.09 m is proposed for the construction. The tunnel will pass through the karst development area in the mileage DXK5 + 400 ~ DXK6 + 400 and QXK5 + 385 ~ QXK6 + 395 sections, totaling about 2,010 m. The buried depth of the tunnel roof is 10–25 m.

According to the geotechnical investigations, Carboniferous, Permian, and Triassic limestones are widely distributed in the site, covered with filling soil, silty clay, and red clay. Dissolution fissures that develop in the limestone, karst caves, and water-eroded grooves are present in the local areas. The average depth of the surface water in the site is about 3 m, and the deepest depth is about 5 m. The main types of groundwater are perched water, fissure water, and karst fracture water. The geological profile of the background project is shown in Figure 2.

*2.2. Karst Development Characteristics.* In order to find out the karst development characteristics in the shield crossing sections, an exploration method combining drilling and geophysical prospecting was adopted. The field exploration shows that the karst development degree of the site is strong, as shown in Figure 3. A total of 739 karst caves were exposed in the exploration, and the karst cavity discovery rate was 76.3%. According to the exploration results, the height of 94.7% of caves is within 7.25 m. The number of caves intruding into the tunnel is large, accounting for 52.4% of the total. The distribution of the distance between caves and the tunnel is relatively discrete, and the distance is mostly within 7.25 m. Shallow caves are mostly half or fully filled, and deep-buried caves are mostly without filling. The filling materials are red clay or gravelly clay. The statistics of caves are shown in Tables 2–4.

## 3. Analysis of Influence of Fully Filled Cave Intruding into Tunnel

The boundary condition and stress state of surrounding rock will be affected when karst caves intrude into the tunnel profile. Therefore, this chapter mainly analyzes the influence of intrusive caves on the stability of the lining and excavation face, and the type of caves that can be nontreated is determined.

*3.1. Analysis of Influence of Intrusive Cave on Lining.* The effect on the lining is greatest when intrusive caves are within the lining range. The boundary conditions of the lining in cave parts are different from the other parts (Figure 4). This will change the surrounding rock pressure that should be evenly distributed on the structure [28, 29].

Among the calculation and evaluation methods of lining safety, there are the load-structure method, stratum-structure method, etc. The stratum-structure model takes into account the self-stabilizing ability of the surrounding rock, and the calculated internal force of the lining is generally smaller. For safety reasons, the influence of intrusive caves on the lining is studied on the basis of the load-structure model.

Table 1: Treatment range of shield tunnel with a diameter of about 6 m.

| Engineering case | Tunnel outer diameter (m) | Karst cave development | Treatment range |
|---|---|---|---|
| Shield tunnel of Guangzhou metro line 9 (data from Qian [14]) | 6 | There are 132 karst caves, including 93 unfilled karst caves, 39 half filled and fully filled karst caves | 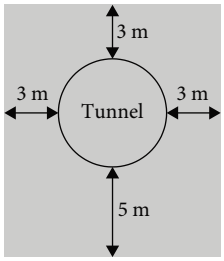 |
| Shield tunnel of Nanning metro line 3 (data from Xie [19]) | 6 | There are 178 karst caves, including five unfilled karst caves, 66 half filled karst caves, and 107 fully filled karst caves | 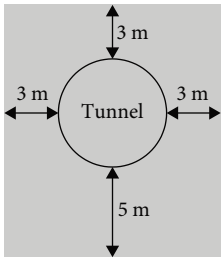 |
| Shield tunnel of Shenzhen metro line 16 (data from Zhang [20]) | 6.2 | There are 258 karst caves, including 220 unfilled karst caves, 38 half filled and fully filled karst caves | 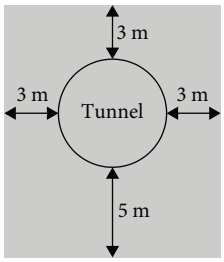 |
| Shield tunnel of Kunming metro line 4 (data from Liu et al. [21]) | 6.2 | There are 219 karst caves, including 44 unfilled and half filled karst caves and 175 fully filled karst caves | 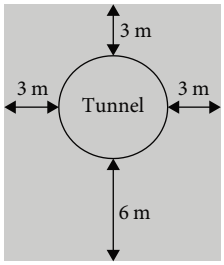 |
| Shield tunnel of Wuhan metro line 27 (data from Zhang [22]) | 6.2 | There are 536 karst caves, including 241 unfilled karst caves, 130 half filled karst caves, and 165 fully filled karst caves | 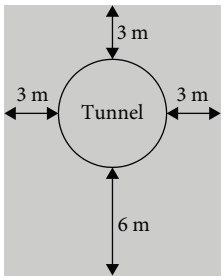 |
| Shield tunnel of Changsha metro line 3 (data from Ma [23]) | 6.2 | There are 89 karst caves, including 14 unfilled karst caves, 75 half filled and fully filled karst caves | 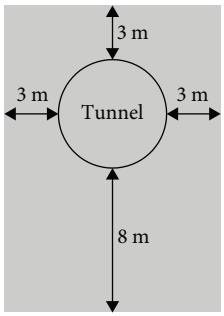 |

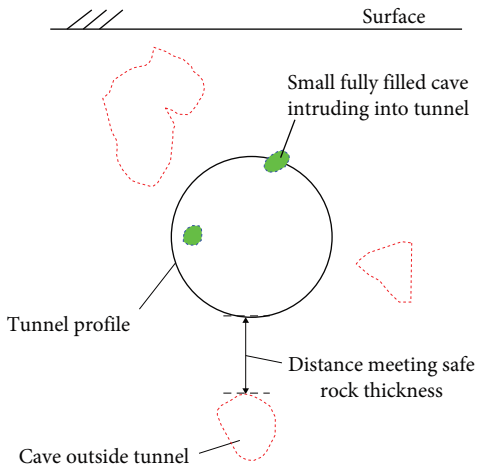


Figure 1: Distribution of karst caves.

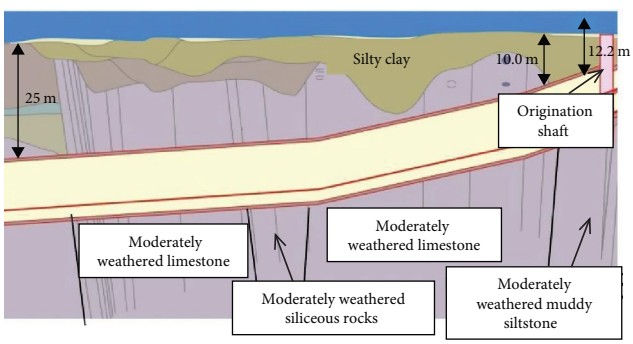


Figure 2: Geological profile.

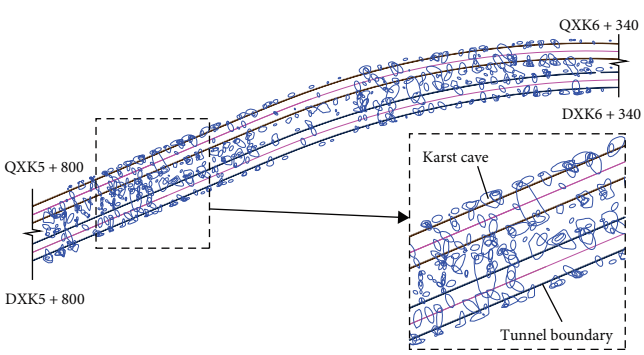


Figure 3: Partial results of karst exploration (DXK5 + 800 ~ DXK6 + 340 and QXK5 + 800 ~ QXK6 + 340).

Table 2: Height of karst cave.

| Height of karst cave $h_c$ (m) | Number of caves | Percentage (%) |
|---|---|---|
| $h_c \leq 3.625$ | 578 | 78.2 |
| $3.625 < h_c \leq 7.25$ | 122 | 16.5 |
| $7.25 < h_c \leq 14.5$ | 31 | 4.2 |
| $h_c > 14.5$ | 8 | 1.1 |

*3.1.1. Calculation Model.* Scholars used the load-structure method to analyze the influence of voids on the internal forces of the lining, removing the loads and constraints of voids behind the lining [30–33]. For the purpose of simulating the condition of caves intruding into the lining range, this study refers to the method and does not set up surrounding rock constraints and loads in a certain part. The calculation model is shown in Figure 4.

Table 3: Spatial relationship between karst cave and tunnel.

| Location of karst cave | Number of caves | Percentage (%) |
|---|---|---|
| Intrude into the tunnel | 387 | 52.4 |
| Within 7.25 m above the tunnel roof | 147 | 19.9 |
| Outside 7.25 m above the tunnel roof | 69 | 9.3 |
| Within 7.25 m below the tunnel floor | 89 | 12.0 |
| Within 7.25–14.5 m below the tunnel floor | 39 | 5.3 |
| Outside 14.5 m below the tunnel floor | 8 | 1.1 |

Table 4: Filled condition of karst cave.

| Filled condition of karst cave | Number of caves | Percentage (%) |
|---|---|---|
| Fully filled | 187 | 25.3 |
| Half filled | 489 | 66.2 |
| Unfilled | 63 | 8.5 |

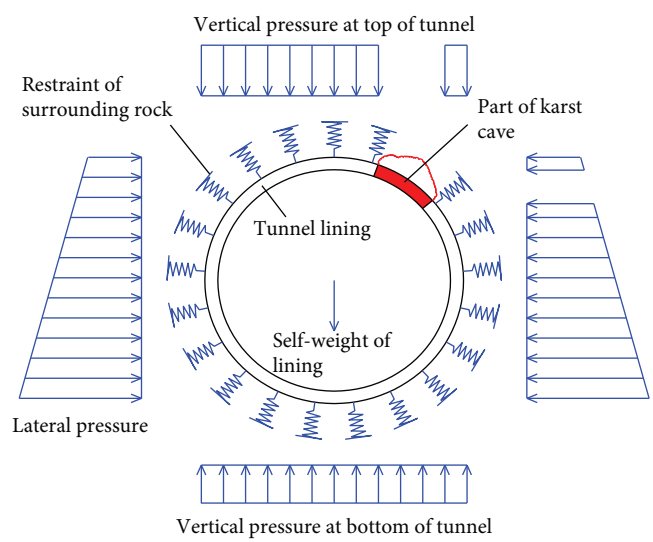


Figure 4: Calculation model of karst cave behind lining.

MIDAS software is applied for the calculation. In the model, the lining is a homogeneous ring, and the basic parameters of the lining are shown in Table 5. Elastic springs are used to simulate the rock reaction to structure, the resistance coefficient of elastic springs is 500 MPa/m, which is taken from the foundation coefficient of the surrounding rock measured by the experiment. The vertical soil pressure at the top of the tunnel is 343.5 kN/m$^2$ (The maximum soil pressure in background engineering), and the lateral pressure coefficient is 0.2.

Considering that the tunnel is undrained, the static water pressure is applied to the lining ring. Due to the nonconnection between karst cave water and surface water in the

Table 5: Basic parameters of lining.

| Outer diameter (m) | Inner diameter (m) | Thickness (m) | Longitudinal width (m) | Unit weight (kN/m$^3$) | Elastic modulus (MPa) | Poisson ratio |
|---|---|---|---|---|---|---|
| 14.5 | 13.3 | 0.6 | 2.0 | 25.0 | 2.76e4 | 0.2 |

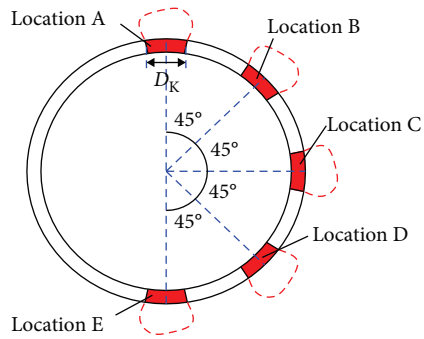


Figure 5: Intrusive positions.

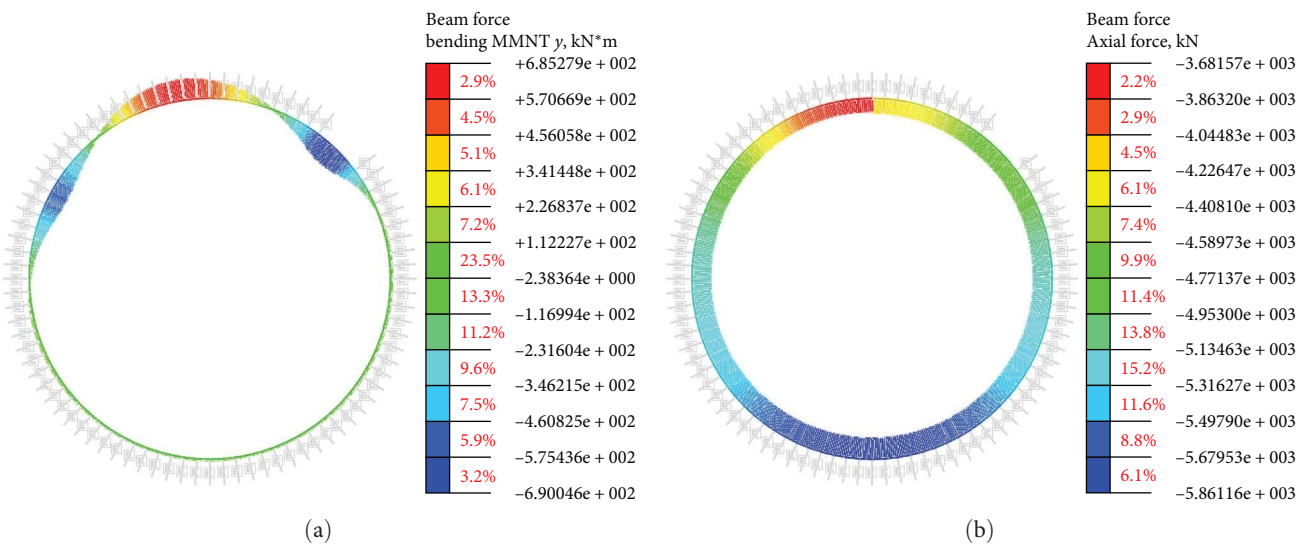


Figure 6: Example of lining internal force (cave at location B): (a) bending moment and (b) axial force.

background project, the cave parts do not add water pressure. The calculation result of lining internal force is larger under this boundary condition, and it is safer for determining the type of caves that can be nontreated. Moreover, the distance between the highest water level and the deepest buried vault is about 30 m in the background project, so the static water pressure is calculated based on this depth.

*3.1.2. Conditions of Analysis.* Intrusive positions are taken at the top, bottom, and side of the tunnel, as shown in Figure 5. The width of the cave parts $D_k$ is 1–4 m.

*3.1.3. Analysis of Calculation Results.* The bending moment and axial force of the lining are calculated by the above model, as shown in Figure 6. The calculation results of the lining bending moment under different intrusive positions and widths are summarized in Figure 7.

As can be seen from Figure 7, when the intrusive cave is located at the position A, the bending moment at the 0° section of the lining (the center of the cave part) changes from negative to positive. And the larger the width of the cave part, the greater the bending moment at the vault. When the intrusive cave is located at position B, the bending moment at the 45° section of the lining (the center of the cave part) does not reverse. As the width of the cave part increases, the bending moment at the 45° section of the lining gradually increases, and the bending moment at the 22.5° and 67.5° sections of the lining decreases first and then increases. If the intrusive cave is located at the positions C, D, and E, the direction of the bending moment at the center of

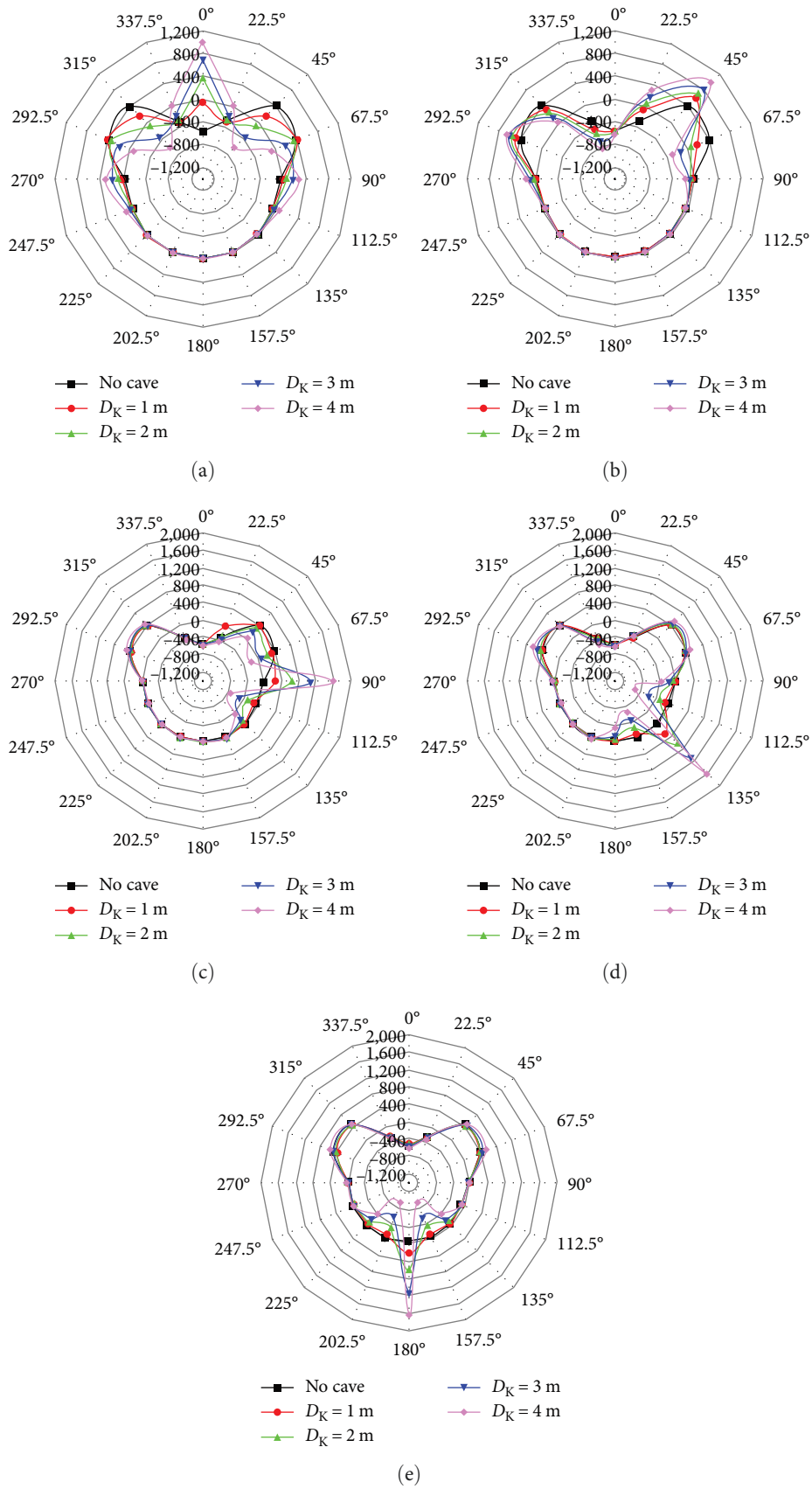


Figure 7: Calculation results of bending moment (the unit in figure is kN·m): (a) location A, (b) location B, (c) location C, (d) location D, and (e) location E.

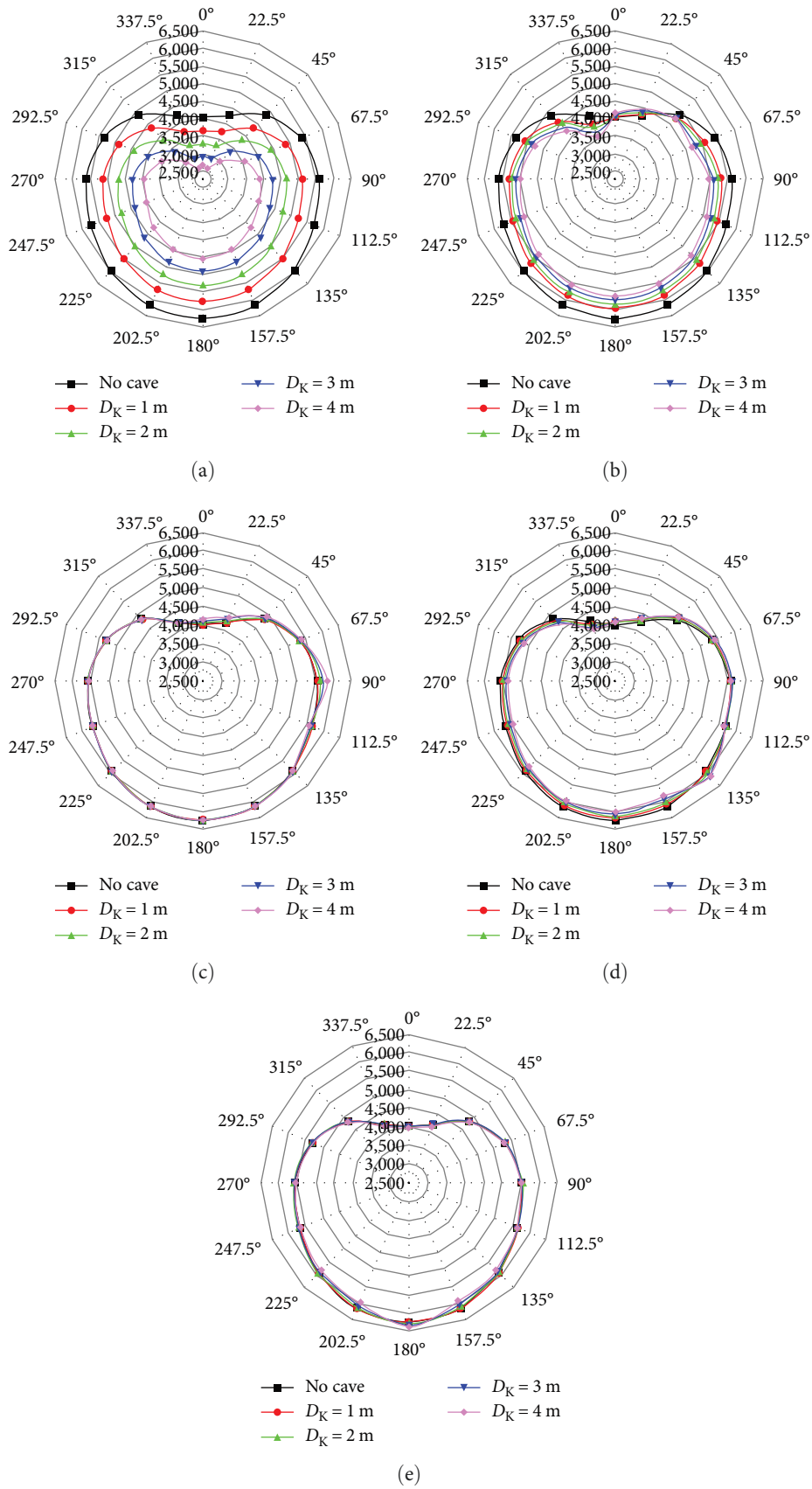


Figure 8: Calculation results of axial force (the unit in figure is kN): (a) location A, (b) location B, (c) location C, (d) location D, and (e) location E.

cave parts changes, and the bending moment distribution of the other parts does not change much. The larger the width of the cave part, the greater the bending moment of the cave part.

According to the calculation results of axial force (Figure 8), if the intrusive cave is located at positions A and B, the axial force of most parts of the lining will decrease with the increase of the width of cave parts. In the case of the intrusive cave at positions C, D, and E, the change in the width of cave parts has a little effect on the axial force of the lining. Considering that the upper part of the lining bears a large vertical water and soil pressure, the stress redistribution caused by the occurrence of caves is more obvious. However, the lower part of the lining mainly bears the resistance of the surrounding rock and the small horizontal water and soil pressure. The appearance of the caves at positions C, D, and E only makes the local stress concentration more obvious but has little effect on the overall axial force of the lining. In conclusion, it can be seen from the calculation results that the lining internal force changes sharply with the width of cave parts exceeding 2 m.

The lining safety coefficient in Chinese standards TB1003 and JTG3370.1 is often used to evaluate the stability of linings [30–33]. It is mainly to check the compressive and tensile strength of axial and eccentric compression members. The calculation formula is as follows:

$$K \geq K_{\mathrm{l}}, \tag{1}$$

where $K$ is the lining safety coefficient, $K_{\mathrm{l}}$ is the limiting value of the lining safety coefficient, taken as 2.4.

For small eccentric compression members ($M/N < 0.2h$), the lining safety coefficient $K$ can be calculated as follows:

$$K = \frac{\varphi \alpha R_{\mathrm{a}} bh}{N}, \tag{2}$$

where $R_{\mathrm{a}}$ is the ultimate compressive strength of the concrete; $N$ is the axial force, $b$ is the section width; $h$ is the section thickness; $\varphi$ is the longitudinal bending factor of the component, $\varphi$ is taken as 1.0 for the tunnel lining; and $\alpha$ is an eccentric influence coefficient of axial force.

For large eccentric compression members ($M/N > 0.2h$), the lining safety coefficient $K$ can be calculated as follows:

$$K = \varphi \frac{1.75 R_{\mathrm{l}} bh}{\frac{6M}{h} - N}, \tag{3}$$

where $R_1$ is the ultimate tensile strength of the concrete, $M$ is the bending moment.

The calculation results of the lining safety coefficient of each condition are shown in Figure 9. No matter where the intrusive caves are located, the lining safety coefficients of the local section in the lining will be reduced. For $D_{\mathrm{k}} = 3$ m, the minimum lining safety coefficient appears at intrusive positions, and the coefficients at each intrusive position are 1.31 (position A), 1.54 (position B), 1.07 (position C), 1.23 (position D), and 1.14 (position E). Compared with the minimum lining safety coefficient of the condition without caves ($K = 3.58$), the coefficients at each intrusive position are reduced by 63.4% (position A), 57.0% (position B), 70.1% (position C), 65.6% (position D), and 68.2% (position E) in the case of $D_{\mathrm{k}} = 3$ m. According to the calculation results (Figure 9), lining safety coefficients are lower than the limit value of standards $K_{\mathrm{l}}$ in the case of $D_{\mathrm{k}} \geq 3$ m, and the lining structure will basically fail at this time, seriously affecting the normal use of the tunnel.

In the condition of $D_{\mathrm{k}} = 2$ m, the minimum lining safety coefficients of each intrusive position are 7.39 (position A), 2.57 (position B), 3.82 (position C), 3.43 (position D), and 3.17 (position E), which are all greater than $K_{\mathrm{l}}$. This indicates that the bearing capacity of the lining also has a certain reserve after the karst caves with $D_{\mathrm{k}} \leq 2$ m intrude.

*3.2. Analysis of Antifracturing Ability for Cave Filling.* The background project will be constructed with a slurry shield, relying on the slurry pressure to resist the water and soil pressure on the excavation face of the slurry shield. If the strength of intrusive cave fillings is too low, the slurry pressure will exceed the antifracturing ability of the fillings, and then soil fracturing will be induced in the intrusive caves (Figure 10). In another aspect, the shield of the background project passes through moderately weathered rock formations whose thickness is great, and strata have a strong self-stabilizing ability. If small fully filled caves are encountered during shield tunneling in moderately weathered rock formations, the influence on the stability of rock mass is limited near the excavation face [34]. In conclusion, the greatest threat to the excavation face is the soil fracturing of cave fillings.

To prevent the occurrence of soil fracturing in fully filled caves during shield tunneling (Figure 10), the antifracturing ability of cave fillings should be evaluated. The common method is to calculate the initial fracturing pressure of the soil and compare it with the slurry pressure on the excavation face [35–37].

In the background project, the cave fillings are mainly plastic clay, and some are flow-soft plastic or hard-plastic red clay. Some physical and mechanical parameters of cave fillings are shown in Table 6. In clay, the initial fracturing pressure $P_{\mathrm{f}}$ can be expressed as follows [35–37]:

$$P_{\mathrm{f}} = \sigma_3 \cdot (1 + \sin \varphi_{\mathrm{c}}) + c \cdot \cos \varphi_{\mathrm{c}}, \tag{4}$$

where $P_{\mathrm{f}}$ is the initial fracturing pressure, $\varphi_{\mathrm{c}}$ is the internal friction angle of the soil, $c$ is the cohesion of the soil, and $\sigma_3$ is the minimum principal stress in the strata.

For the shallow cover, $\sigma_3$ should be calculated as follows:

$$\sigma_3 = (\gamma Z + q) \cdot (1 - \sin \varphi_{\mathrm{c}}), \tag{5}$$

where $\gamma$ is the unit weight of the rock or soil layer, $Z$ is the overburden thickness, and $q$ is the surcharge load.

The shield tunnel of the background project will be mainly excavated in moderately weathered rock formations

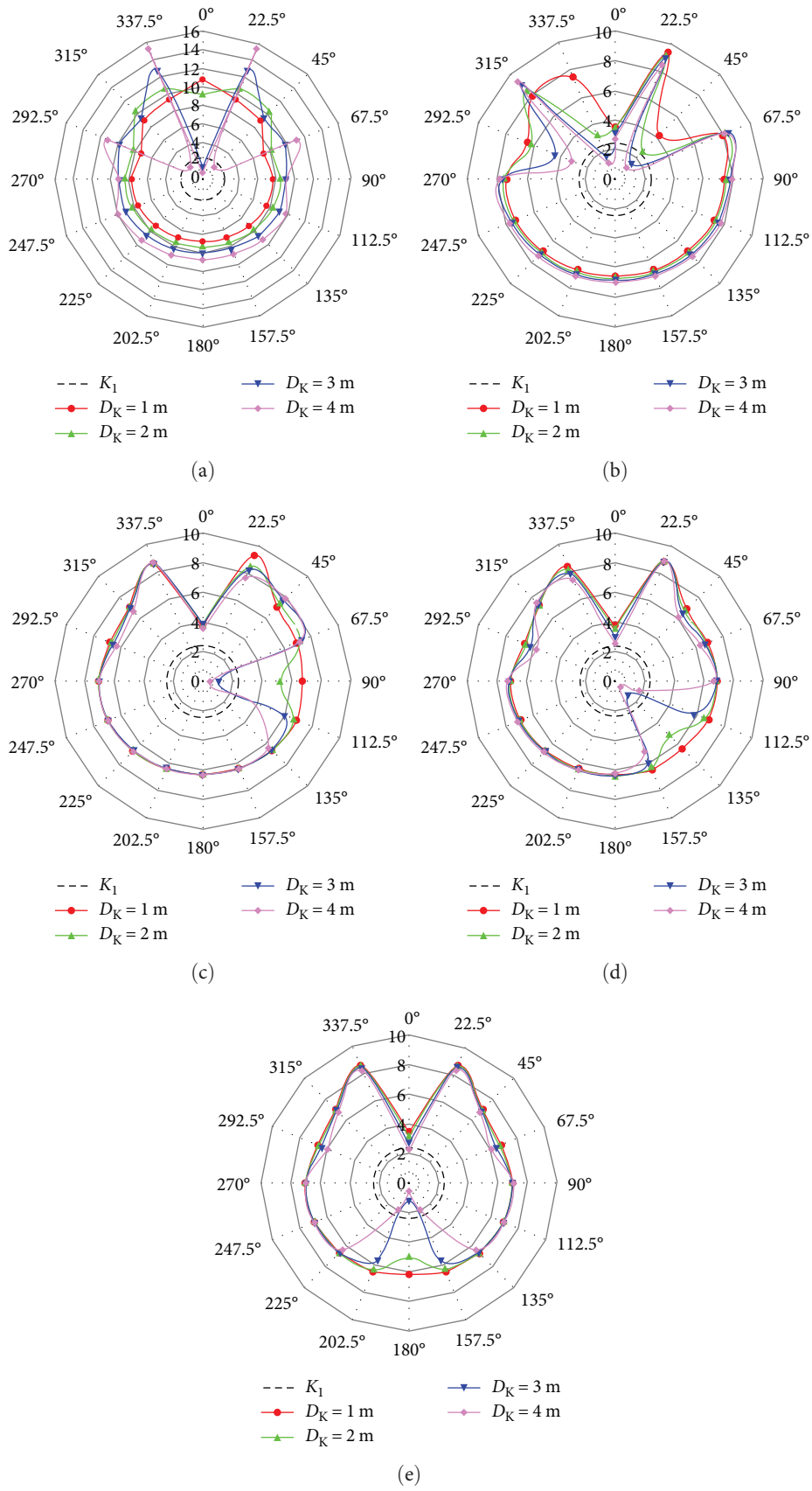


Figure 9: Calculation results of lining safety coefficient: (a) location A, (b) location B, (c) location C, (d) location D, and (e) location E.

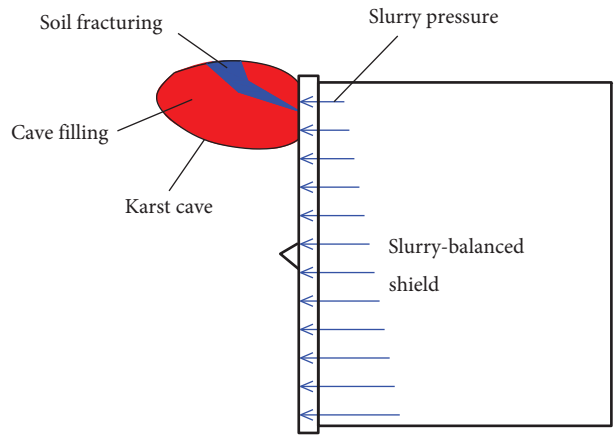


Figure 10: Soil fracturing in intrusive cave.

Table 6: Physical and mechanical parameters of cave filling.

| Cave filling | Internal friction angle (degree) | Cohesion (kPa) | Liquidity index | Plasticity index |
|---|---|---|---|---|
| Flow-soft plastic clay | 4.0 | 7.0 | 1.41 | 27.1 |
| Plastic clay | 11.0 | 43.0 | 0.45 | 25.7 |
| Hard plastic clay | 16.5 | 59.0 | 0.07 | 23.4 |

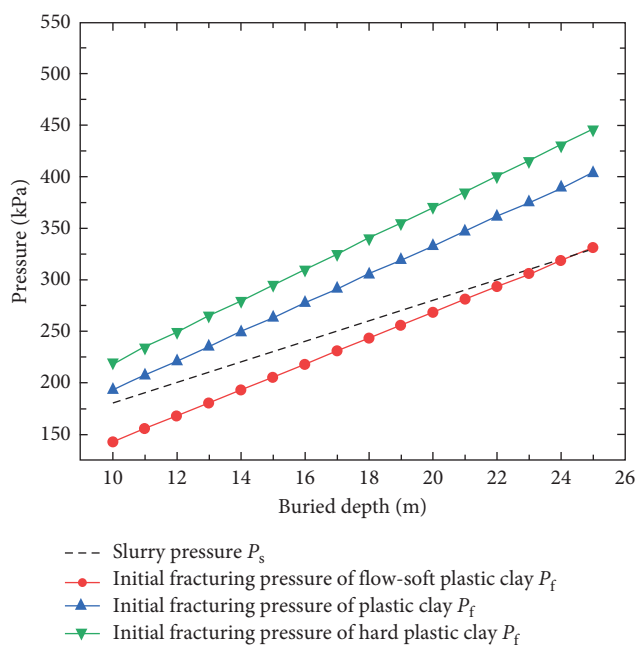


Figure 11: Calculation results of initial fracturing pressure and slurry pressure.

under the lake. Due to the self-stabilizing ability of moderately weathered rock and larger water pressure, the slurry pressure is generally not necessary to consider the soil pressure on the excavation face for the case of the background project [37, 38]. Therefore, the slurry pressure $P_s$ can be calculated as follows [37]:

$$P_S = \gamma_w Z_w + P_a, \tag{6}$$

where $\gamma_w$ is the unit weight of water, $Z_w$ is the depth of the water table, $P_a$ is the prereservation pressure, generally taken as 10–30 kPa [38], and $P_a$ is taken as 30 kPa for the case of this paper.

The condition of the tunnel buried depth of 10–25 m is selected to calculate the initial fracturing pressure of cave fillings and slurry pressure at intrusive positions. The results are shown in Figure 11. It is clear that the slurry pressure

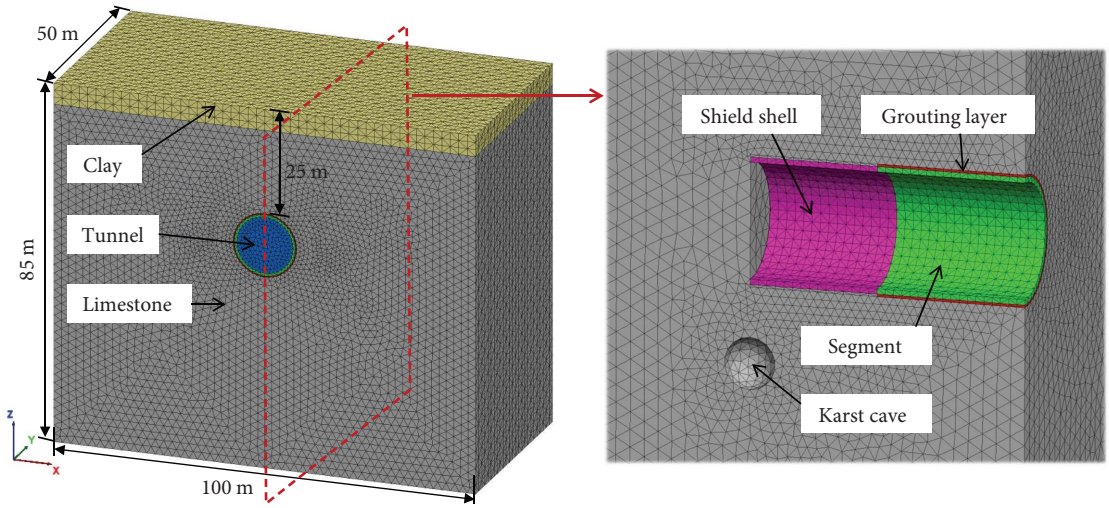


Figure 12: Simulation model.

Table 7: Calculation parameters of various materials.

| Material | Elastic modulus (MPa) | Poisson ratio | Unit weight (kN/m$^3$) | Internal friction angle (degree) | Cohesion (kPa) |
|---|---|---|---|---|---|
| Clay | 13.0 | 0.45 | 20.3 | 16.0 | 45.0 |
| Limestone | 10,700.0 | 0.30 | 24.0 | 44.0 | 1,100.0 |
| Shield shell | 200,000.0 | 0.26 | 131.3 | — | — |
| Segment | 27,600.0 | 0.20 | 25.0 | — | — |
| Grouting layer | 5.0 | 0.30 | 17.0 | — | — |

exceeds the initial fracturing pressure of the flow-soft plastic clay, so it is recommended to reinforce the caves filled with the flow-soft plastic clay.

*3.3. Fully Filled Cave without Treatment.* According to the conclusion drawn by Li and Yan [34], when the size of fully filled caves in front of the excavation face is less than 0.25$D$ ($D$ is the outer diameter of the tunnel), the stability of the rock mass near the excavation face is little affected. Through the analysis of the effects of intrusive caves, the fully filled caves with a size of not more than 2 m have a little influence on the lining safety, and the fillings of the plastic or hard plastic clay have sufficient antifracturing ability. Therefore, the fully filled caves with a size of not more than 2 m and filled with plastic or hard plastic clay have less threat to the tunnel.

Considering that the taking values in the calculation are conservative for safety reasons, and the strengthening measure such as wall-back grouting will be conducted during tunneling, the fully filled caves of the above type can be left unreinforced.

## 4. Analysis of Safe Distance between Tunnel and Cave outside Tunnel

The treatment range outside the tunnel can be determined by the critical safe distance [39]. In this paper, the critical safe distance between a super-large diameter shield tunnel and karst caves in different directions is solved by a 3D numerical simulation to determine the treatment range outside the tunnel.

*4.1. Simulation Model.* According to the geological conditions of the background project, a 3D simulation model is established whose length, width, and height are 100, 50, and 85 m, respectively (Figure 12). The geometry of the model is defined by the following sizes: the thickness of the clay is 5 m, the thickness of the underlying limestone is 80 m, the distance between the tunnel roof and the surface is 25 m, the outside diameter of the lining is 14.5 m, and the outside diameter of the shield shell is 15.09 m. The height of the surface water level is 5 m. All the side boundaries are restrained in the normal direction. The bottom boundary is fixed and the top boundary is free. The karst cave is simplified as a sphere based on experience [9, 39], and there are no fillings in the simulated caves for safety reasons.

The steps of the simulated construction process are as follows: (1) excavate the rock mass in the karst cave after modeling, (2) calculate the self-weight stress field of the model, and (3) excavate the tunnel and simulate the lining, shield shell, and grouting layer. After each step, the model is solved immediately until the ratio of the maximum difference between the external force and the internal force of all the gridpoints to the average applied force is less than $10^{-5}$.

In modeling, the rock and soil mass, lining, shield shell, and grouting layer are all solid elements. First, the Mohr–Coulomb

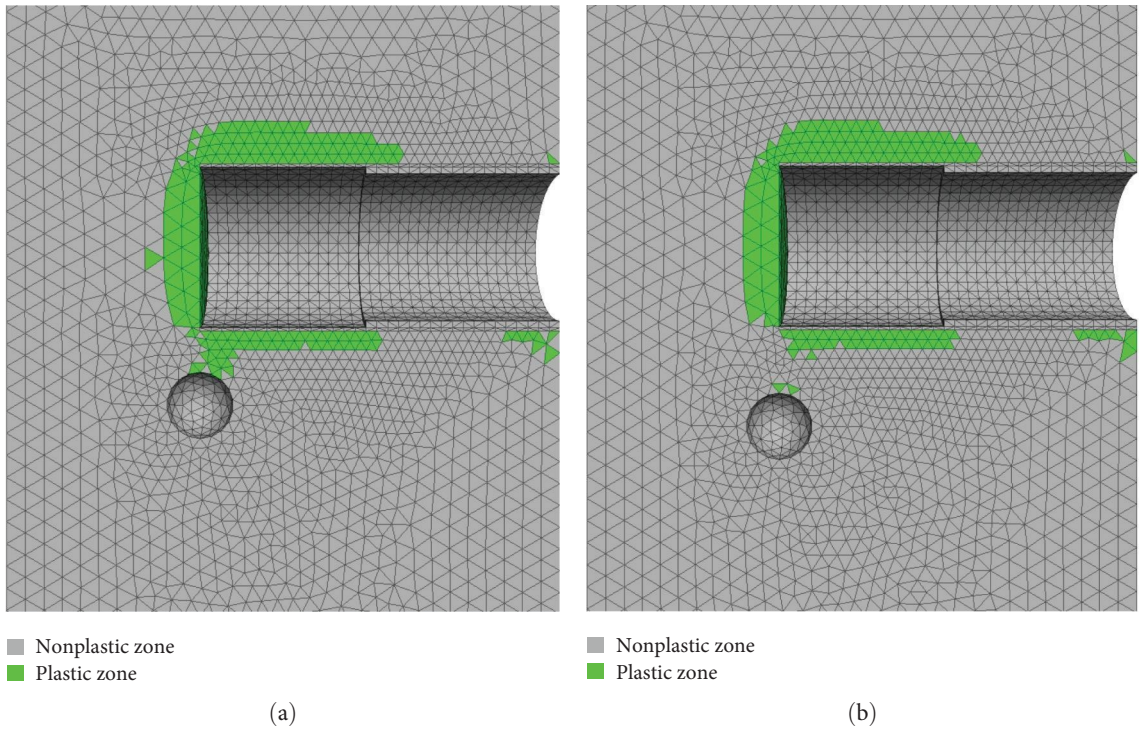


Figure 13: Numerical simulation example of a cave located under the tunnel: (a) run-through of plastic zone and (b) non run-through of plastic zone.

Table 8: Critical safe distance of numerical simulation.

| Location of karst cave | Diameter of caves (m) | Critical safe distance (m) |
|---|---|---|
| Upper part of tunnel | 3.0 | 1.0 |
| | 4.5 | 1.0 |
| | 6.0 | 1.5 |
| | 7.5 | 2.0 |
| | 9.0 | 2.5 |
| Lateral part of tunnel | 3.0 | 2.0 |
| | 4.5 | 2.0 |
| | 6.0 | 2.5 |
| | 7.5 | 3.5 |
| | 9.0 | 4.0 |
| Lower part of tunnel | 3.0 | 2.0 |
| | 4.5 | 2.5 |
| | 6.0 | 3.0 |
| | 7.5 | 4.5 |
| | 9.0 | 6.0 |

elastic-perfectly plastic model is adopted for all solid elements during calculating the self-weight stress field of the simulation model, and the calculation parameters are obtained from the physical parameters of rock and soil mass. After that, the displacement and plastic zone of the simulation model are cleared, and then the rock inside the shield shell and the lining are excavated. Meanwhile, the solid elements of the lining, shield shell, and grouting material are all changed to isotropic elastic model elements, and new calculation parameters are given in

Table 9: Treatment range outside the tunnel.

| Location of cave | Size of largest cave (m) | Distance between tunnel and treatment range (m) |
|---|---|---|
| Upper part of tunnel | 15.73 | 5.25 |
| Lateral part of tunnel | 13.12 | 5.88 |
| Lower part of tunnel | 14.08 | 13.81 |

these elastic model elements for simulating the construction process. For this step, the weight of the shield machine is converted to the weight of shield shell elements. The lining is treated as a homogeneous ring, and the stiffness of the lining material is reduced by 40% considering the influence of joints. The parameters of the grouting layer are valued in the condition of incomplete hardening. The calculation parameters of various materials are shown in Table 7. The slurry pressure is applied to the excavation during simulation, and its value is calculated according to Equation (6).

*4.2. Determination of Critical Safe Distance.* The critical safe distance between the tunnel and caves is essentially the critical rock thickness of rock mass instability. In numerical tests, the instability criterion is often needed to indicate that the rock mass is in the limit equilibrium state. In many studies, the run-through of the plastic zone between the tunnel and caves was taken as the basis for instability [8, 9, 18, 19]. In order to obtain the critical safe distance in this paper, the distance between the shield tunnel and caves is continuously adjusted until the plastic zone is run-through, as shown in Figure 13.

*4.3. Test Scheme and Simulation Results.* The caves in the model are located at the upper, lateral, and lower parts of the tunnel. The critical safe distance is solved in the context of the caves with a diameter of 3.0–9.0 m, and the results are shown in Table 8.

By the regression analysis of the critical safe distance in Table 8 and considering the safety factor, the calculation formula of treatment range outside the tunnel is obtained as follows:

$$\begin{cases} H_U = 0.24095 \cdot k_c \cdot D_c^{1.05177} \\ H_S = 0.71121 \cdot k_c \cdot D_c^{0.74957} \\ H_L = 0.32898 \cdot k_c \cdot D_c^{1.34401} \end{cases}, \quad (7)$$

where $H_U$ is the treatment range in the upper part of the tunnel, $H_s$ is the treatment range in the lateral part of the tunnel, $H_L$ is the treatment range in the lower part of the tunnel, $k_c$ is the safety factor of the treatment range, it is taken as 1.2 [39], and $D_c$ is the size of the cave.

*4.4. Outside Cave without Treatment.* According to the cave size of the background project, the treatment range of caves outside the tunnel is calculated based on Equation (7), and the results are shown in Table 9. The obtained treatment range outside the tunnel is close to similar projects that have been built [10, 24, 39]. The caves outside the calculated distance in Table 9 can be left unreinforced.

In addition, the critical safe distance in Table 8 is only 1–2 m for the caves with a size of 3 m. Therefore, the caves with a size of less than 3 m can be left unreinforced when the distance between the tunnel and the caves is greater than 3 m. This treatment concept has also been applied in the project of Dalian metro line 5 [24].

## 5. Determination of Treatment Range

The fully filled caves with a size of less than 2 m and filled with plastic or hard plastic clay can be left unreinforced through the analysis of the effects of intrusive caves. On the other hand, caves that meet the critical safe distance can be left unreinforced.

In addition, the surrounding rock at the bottom of the tunnel bears the weight of the shield machine, and its stability is highly required during the construction process. As a result, it is considered that the karst caves in a certain range under the tunnel must be reinforced.

In summary, according to the analysis results of this paper, combined with the experience of shield engineering and karst treatment in Wuhan [15, 16, 18], the treatment range is determined for a super-large diameter shield tunnel located in the strong karst development area (Figure 14). The proposed treatment range follows the principle of divisional processing on the basis of refining the common treatment range. The specific requirements for the treatment range of Figure 14 are as follows:

(1) In area A, the fully filled caves with a size of less than 2 m and filled with plastic or hard plastic clay can be left unreinforced. Other caves intruding into area A must be reinforced.

(2) Caves intruding into area B must be reinforced.

(3) In area C, caves with a size of less than 3 m can be left unreinforced. Caves with a size of greater than 3 m and intruding into area C must be reinforced.

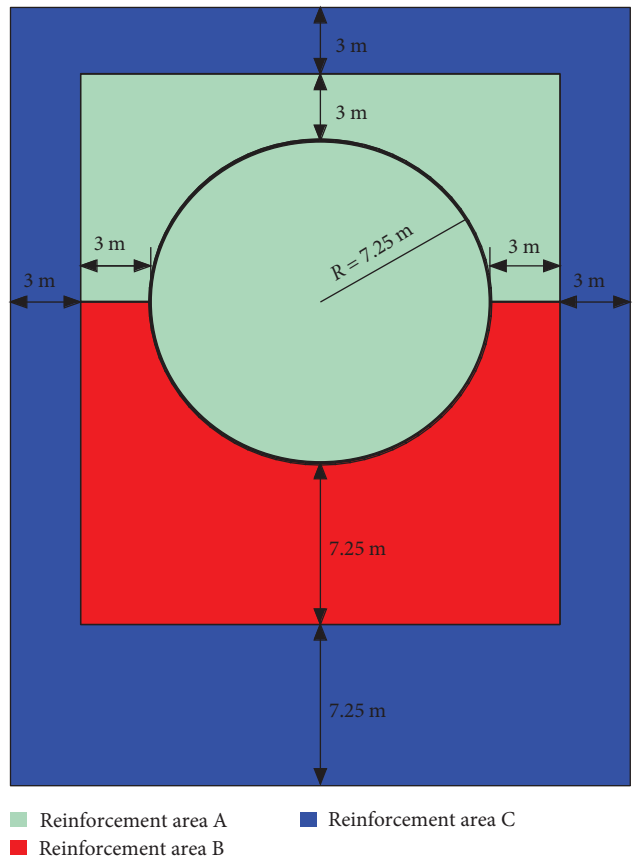


Figure 14: Treatment range of background project.

## 6. Conclusions

Based on a karst treatment project of a super-large diameter shield tunnel located in a strongly karst-developed area, this paper analyzes the influence of intrusive fully filled caves on the stability of the lining and excavation face. The calculation formula for the critical safe distance between the tunnel and caves outside the tunnel is proposed. The corresponding treatment range is proposed, and the following conclusions are obtained:

(1) The stress state of the lining will be changed when karst caves intrude into the tunnel. The direction of the lining bending moment at the center of the intrusive position changes in the condition of intrusive caves located in the vault and lower part of the lining. And the larger the width of cave parts, the greater the lining bending moment at intrusive positions. Intrusive karst caves at the lower part of the tunnel have a

relatively small effect on the lining axial force. When the size of the intrusive cave part exceeds 2 m, the lining internal force changes sharply.

(2) The influence analysis of intrusive fully filled caves on the stability of the excavation face is conducted by means of the analysis of the slurry fracturing for fillings. The slurry pressure exceeds the initial fracturing pressure of the flow-soft plastic clay, so it is recommended to reinforce the intrusive caves filled with the flow-soft plastic clay. According to simulation results, the critical safe distance is only 1–2 m for the outside caves with a size of 3 m. Therefore, the caves with a size of less than 3 m can be left unreinforced when the distance between the tunnel and the cave is greater than 3 m.

(3) The treatment range is determined for a super-large diameter shield tunnel located in the strongly karst-developed area. The obtained treatment range is close to the similar projects that have been built, indicating that analysis results are reasonable. The treatment range follows the principle of divisional processing, and the types of treated caves in different treatment zones are different. The common treatment range is refined in this paper.

## Data Availability

The data used to support the findings of this study are available from the corresponding author upon request.

## Conflicts of Interest

The authors declare that they have no conflicts of interest in this work.

## Acknowledgments

The authors would like to acknowledge financial support from the Research and Development Project of Ministry of Housing and Urban-Rural Development, China (K20200533), the Development Program of Scientific and Technological Research of China Railway 16th Bureau Group Co., Ltd. (K2019-39C, K2019-23C, K2020-15, and K2021-18C).

## References

[1] W. B. Zhu, H. Zhang, and H. Huang, "Analysis of and prevention countermeasures for underground engineering risks in red bed areas with developed karst," *Modern Tunnelling Technology*, vol. 58, no. 5, pp. 179–186 212, 2021.

[2] S. Q. Sun, L. P. Li, J. Wang, S. G. Song, P. He, and Z. G. Fang, "Reconstruction and measurement of irregular karst caves using BLST along the Shield Metro Line," *Applied Sciences*, vol. 10, no. 1, Article ID 392, 2020.

[3] J. Wang, L. Li, S. Shi, S. Sun, X. Ba, and Y. Zhang, "Fine exploration and control of subway crossing karst area," *Applied Sciences*, vol. 9, no. 13, Article ID 2588, 2019.

[4] W.-C. Cheng, Q.-L. Cui, J. Shen, A. Arulrajah, and D.-J. Yuan, "Fractal prediction of grouting volume for treating karst caverns along a shield tunneling alignment," *Applied Sciences*, vol. 7, no. 7, Article ID 652, 2017.

[5] K. R. Hong, Y. L. Du, K. Chen, H. H. Feng, L. H. Jia, and F. Xu, "Full-face tunnel boring machines (shields/TBMs) in China: history, achievements, and prospects," *Tunnel Construction*, vol. 42, no. 5, pp. 739–756, 2022.

[6] W. Zhang, J. Qi, G. Zhang et al., "Full-scale experimental study on failure characteristics of the key segment in shield tunnel with super-large cross-section," *Tunnelling and Underground Space Technology*, vol. 129, Article ID 104671, 2022.

[7] N. Yoshito and K. Naoki, "Super large diameter muddy soil shield machine for road tunnel," *Journal of IHI Technologies*, vol. 50, no. 2, pp. 69–78, 2010.

[8] S. Q. Sun, *Precise Characteristics of Irregular Cavity and Its Effect on Surrounding Rockmass Stability of Shield Tunnel*, Shandong University, Jinan, China, 2019.

[9] Q. W. Liu, S. Q. Sun, H. B. Wang, J. X. Dong, and H. C. Hu, "A calculation method for safety distance between the confined karst cave and the shield tunnel based on upper bound theorem," *Geotechnical and Geological Engineering*, vol. 38, no. 6, pp. 6587–6599, 2020.

[10] H. B. Li, F. Jia, J. Li, and S. B. Li, "Key technologies for design of subsea tunnel of Dalian metro line 5," *Rock and Soil Mechanics*, vol. 38, no. S1, pp. 395–401, 2017.

[11] Y. K. Long, *The Study of Stability and Processing Technology of Karst Caves in Changsha Metro Line 1*, Central South University, Changsha, China, 2021.

[12] G. T. Li, "Design of karst treatment: case study on north extension section of no. 3 line of Guangzhou metro," *Tunnel Construction*, vol. 29, no. 1, pp. 61–64 87, 2009.

[13] Z. Qian, Y. S. Xu, S. L. Shen, and Q. L. Cui, "A case study of ground surface grouting reinforcement of shield tunnel in karst strata with sandy soil cover," *Tunnel Construction*, vol. 36, no. 4, pp. 479–484, 2016.

[14] Z. Qian, *Environmental Impacts due to Shield Tunneling in Karst Region Covered with Sandy Strata*, Shanghai Jiao Tong University, Shanghai, China, 2016.

[15] X. Y. Zhuo, "Countermeasures for the shield tunnel passing through the karst area overlying soft plastic red clays," *Modern Tunnelling Technology*, vol. 56, no. 6, pp. 96–202, 2019.

[16] S. K. Li and L. Tao, "Features of karst development in Wuhan area and treatment of karsts encountered in construction of Wuhan metro," *Tunnel Construction*, vol. 35, no. 5, pp. 449–454, 2015.

[17] Y. S. Liu, "Research on the key technology of Changsha metro cross-river tunnel through karst stratum," *Journal of Railway Engineering Society*, vol. 37, no. 6, pp. 76–80, 2020.

[18] W. Wang, S. M. Gao, L. F. Liu, W. S. Wen, P. Li, and J. P. Chen, "Analysis on the safe distance between shield tunnel through sand stratum and underlying karst cave," *Geosystem Engineering*, vol. 22, no. 2, pp. 81–90, 2018.

[19] Q. Xie, *Study on Safety Distance between Tunnel and Karst Cave and Treatment Technology of Cave*, Guangxi University, Nanning, China, 2017.

[20] Z. Zhang, *Study on the Influence Characteristics and Treatment Methods of Karst Cave on the Safety of Shield Tunneling*, Shandong University, Jinan, China, 2021.

[21] W. Liu, F. Y. Liu, D. Peng, X. Zhang, and W. H. Yang, "Karst characteristics and governance measures in Kunming metro line 4," *Journal of Engineering Geology*, vol. 26, no. s1, pp. 202–207, 2018.

[22] M. C. Zhang, "Treatment measures of metro shield tunnel in red clay karst area," *Geotechnical Engineering Technique*, vol. 34, no. 4, pp. 201–205, 2020.

[23] F. D. Ma, "An approach to some key technologies of shield tunnel construction in karst development area under river bottom," *Railway Standard Design*, vol. 62, no. 1, pp. 93–98, 2018.
[24] H. G. Zhou and Y. T. He, "Key technologies for investigation, design and treatment of submarine karst shield tunnel: a case study of railway station-Suoyu station submarine tunnel on Dalian metro line 5," *Tunnel Construction*, vol. 38, no. 11, pp. 1830–1835, 2018.
[25] Z. H. Fang, *Study on Deformation Law of Surrounding Rock of Shield Machine Passing through Filling Cave*, Shandong University, Jinan, China, 2019.
[26] Q. Pan, Q. Z. Zhang, J. L. Zhao, Y. T. He, and S. B. Li, "Analysis on influence of karst distribution on stability of shield tunnels," *Modern Tunnelling Technology*, vol. 55, no. S2, pp. 466–474, 2018.
[27] W. M. Li, H. Ren, Z. M. Li, X. D. Shi, and Y. W. Zhang, "Research on the lining deformation mechanism of tunnel shielding in complex karst stratum," *Journal of Railway Engineering Society*, vol. 35, no. 9, pp. 67–74, 2018.
[28] M. A. Meguid and H. K. Dang, "The effect of erosion voids on existing tunnel linings," *Tunneling and Underground Space Technology*, vol. 24, no. 3, pp. 278–286, 2009.
[29] J. Wang, H. Huang, X. Xie, and A. Bobet, "Void-induced liner deformation and stress redistribution," *Tunnelling and Underground Space Technology*, vol. 40, pp. 263–276, 2014.
[30] G. G. Ying, *Study on Affecting Mechanism of Tunnel Structure-System Safety with Voids behind Lining*, Beijing Jiaotong University, Beijing, China, 2016.
[31] G. G. Ying, D. L. Zhang, L. P. Chen, Q. Fang, and C. P. Zhang, "Amendment of load-structure model with voids behind tunnel lining at vault," *China Civil Engineering Journal*, vol. 48, no. S1, pp. 181–185, 2015.
[32] H. B. Yin, Z. C. Liu, and Y. F. Guo, "Analysis of stress characteristics of lining structure under the influence of combined defects," *Journal of Railway Science and Engineering*, vol. 17, no. 8, pp. 2037–2045, 2020.
[33] Y. C. Ye, L. M. Peng, M. F. Lei, and Y. X. Lin, "Safety analysis of tunnel structures with different patterns of voids behind lining," *Journal of Railway Science and Engineering*, vol. 15, no. 11, pp. 2875–2883, 2018.
[34] J. k. Li and Z. J. Yan, "Analysis on the impact of front karst cave on shield tunneling: a case study of the Hou Hou interval project of Dalian metro line 5," *Science Technology and Engineering*, vol. 20, no. 14, pp. 5798–5804, 2020.
[35] X.-Y. Liu and D.-J. Yuan, "An in-situ slurry fracturing test for slurry shield tunneling," *Journal of Zhejiang University-Science A*, vol. 15, no. 7, pp. 465–481, 2014.
[36] X. Y. Liu and D. J. Yuan, "Setting of slurry pressure without soil fracture during shield tunneling," *China Civil Engineering Journal*, vol. 47, no. 5, pp. 128–132, 2014.
[37] X. Y. Liu, F. M. Wang, D. J. Yuan, H. Y. Fang, and S. L. Zhang, "Range of support pressures for slurry shield and analysis of its influence factors," *Chinese Journal of Geotechnical Engineering*, vol. 41, no. 5, pp. 908–917, 2019.
[38] X. T. Fang, H. W. Tong, J. Yuan, J. X. Xie, and Y. H. Wang, "Calculation model of mud tank pressure and total thrust of mud-water balance shield machine in sand and limestone strata," *Science Technology and Engineering*, vol. 19, no. 12, pp. 288–297, 2019.
[39] H. Shu, Y. Y. Peng, M. Song, S. G. Liu, J. S. Yang, and C. Zhang, "Reasonable reinforcement range of surface grouting for super large diameter shield tunnel through karst development area," *Science Technology and Engineering*, vol. 21, no. 25, pp. 10948–10955, 2021.